The Astronomical Journal, 168:127 (12pp), 2024 September https://doi.org/10.3847/1538-3881/ad58be

A Volume-limited Radio Search for Magnetic Activity in 140 Exoplanets with the Very Large Array

Kevin N. Ortiz Ceballos[1], Yvette Cendes[1,2], Edo Berger[1], and Peter K. G. Williams[1]
[1] Center for Astrophysics | Harvard & Smithsonian, 60 Garden St, Cambridge, MA 02138, USA
[2] Department of Physics, University of Oregon, Eugene, OR 97403, USA
Received 2024 April 25; revised 2024 June 8; accepted 2024 June 13; published 2024 August 22

Abstract

We present results from a search for radio emission in 77 stellar systems hosting 140 exoplanets, predominantly within 17.5 pc using the Very Large Array (VLA) at 4–8 GHz. This is the largest and most sensitive search to date for radio emission in exoplanetary systems in the GHz frequency range. We obtained new observations of 58 systems and analyzed archival observations of an additional 19 systems. Our choice of frequency and volume limit is motivated by radio detections of ultracool dwarfs (UCDs), including T dwarfs with masses at the exoplanet threshold of $\sim$13 M_J. Our surveyed exoplanets span a mass range of $\approx 10^{-3}$–10 M_J and semimajor axes of $\approx 10^{-2}$–10 au. We detect a single target—GJ 3323 (M4) hosting two exoplanets with minimum masses of 2 and 2.3 $M_\oplus$—with a circular polarization fraction of $\approx$40%; the radio luminosity agrees with its known X-ray luminosity and the Güdel–Benz relation for stellar activity suggesting a likely stellar origin, but the high circular polarization fraction may also be indicative of star–planet interaction. For the remaining sources our 3σ upper limits are generally $L_\nu \lesssim 10^{12.5}$ erg s^{-1} Hz^{-1}, comparable to the lowest radio luminosities in UCDs. Our results are consistent with previous targeted searches of individual systems at GHz frequencies while greatly expanding the sample size. Our sensitivity is comparable to predicted fluxes for some systems considered candidates for detectable star–planet interaction. Observations with future instruments such as the Square Kilometre Array and Next-Generation VLA will be necessary to further constrain emission mechanisms from exoplanet systems at GHz frequencies.

Unified Astronomy Thesaurus concepts: Star-planet interactions (2177); Exoplanets (498); Planetary magnetospheres (997); Magnetospheric radio emissions (998); Non-thermal radiation sources (1119)

1. Introduction

Observational constraints on the magnetic activity of exoplanets are extremely limited. While the magnetic fields of all magnetized solar system planets have been measured directly via astronomical observations or in situ measurements (Stevenson 2003), no confirmed direct detection of a magnetic field has been achieved for an exoplanet. Several techniques exist for indirectly estimating the magnetic field strength of exoplanets. Observations of star–planet interactions have been used to constrain exoplanet magnetic fields, for example by identifying modulations in Ca II chromospheric emission from the star in phase with the planetary orbit (Shkolnik et al. 2003, 2005; Gurdemir et al. 2012; Cauley et al. 2019), as well as periodic X-ray emission in phase with the orbital period (Acharya et al. 2023). Transit observations of atmospheric bow shocks (Cauley et al. 2019) and evaporating atmospheres (Ben-Jaffel et al. 2021; Schreyer et al. 2023) have also been used to estimate planetary magnetic fields. However, these methods are indirect and can lead to uncertain estimates.

In the solar system, radio observations serve as direct probes of the magnetic fields of the giant planets (Burke & Franklin 1955; Zarka et al. 1997). The solar system planets emit radiation at radio frequencies through the electron cyclotron maser instability (ECMI) mechanism, which causes emission up to a maximum frequency directly proportional to the maximum magnetic field strength (Zarka 1998). The nonthermal, incoherent gyrosynchrotron process is also present in Jupiter's radio emission, but it is a much weaker signature due to its inefficiency (Zarka et al. 2015), making ECMI measurements the strongest diagnostic of planetary magnetic fields in the solar system.

Searches for radio emission from exoplanet systems, across MHz–GHz frequencies, have so far yielded nondetections (e.g., Winglee et al. 1986; Zarka et al. 1997; Bastian et al. 2000; Lazio et al. 2004; Lazio & Farrell 2007; Lazio et al. 2009; Lynch et al. 2017; O'Gorman et al. 2018; Route 2019; Cendes et al. 2021; Route & Wolszczan 2023) or tentative detections (e.g., Lecavelier des Etangs et al. 2011, 2013). In general, the detection of stellar emission at radio frequencies is still challenging. While the very closest stars are sometimes detectable in their thermal emission (e.g., α Centauri; Trigilio et al. 2018), these are exceptions due to their extremely close distances. Rather, stars are often observable in the radio due to nonthermal emission, such as cyclotron masers and gyrosynchrotron radiation (Dulk 1985), a variable type of emission found across a large portion of the radio spectrum (Hughes et al. 2021). Recently, nontargeted searches through source-location cross-matching on radio sky surveys have permitted new discoveries of radio-bright main-sequence stars at MHz (Callingham et al. 2021; Gloudemans et al. 2023) and GHz (Driessen et al. 2023) frequencies. However, there is not yet evidence that these signals are definitively tied to exoplanets in these systems. A recent promising detection of flaring 2–4 GHz radio emission from YZ Ceti, which hosts a short-period planet, may be coperiodic with the planet's orbit, potentially indicating star–planet interaction (Pineda & Villadsen 2023). A similar

result had also been tentatively presented earlier for Proxima Centauri b (Pérez-Torres et al. 2021)

Searches that have sought to find emission directly from exoplanets (as opposed to from star–planet interactions) have more recently focused on the MHz regime. Jupiter's ECMI emission, caused by its 14 G magnetic field, reaches a maximum cyclotron frequency of about 40 MHz (Zarka et al. 2012). An exoplanet with a magnetic field similar to Jupiter, or up to a few times stronger, would still emit at tens or hundreds of MHz. Two results in this regime have so far been presented as tentative detections. A potential signal from the Tau Bootis system (Turner et al. 2021) was detected with LOFAR but was seen only once and could not be ruled out as being of stellar origin; follow-up observations showed no sign of emission (Turner et al. 2024). Another signal, from the direction of GJ 1151, has also been reported from LOFAR data (Vedantham et al. 2020), but follow-up radial-velocity measurements rule out the presence of a Jupiter-mass companion (Pope et al. 2020). Later observations revealed a long-period ($P = 390$ days) exoplanet, likely too low mass ($M_p \sin i = 10.62\, M_\oplus$) to be the source of the signal (Blanco-Pozo et al. 2023). Further LOFAR detections of circular polarization in a subset of M dwarfs have been likewise attributed to exoplanet interactions (Callingham et al. 2021), although all but two of these newly detected sources are not known to host exoplanets.

On the other hand, GHz frequency radio observations of very low-mass stars and brown dwarfs (hereafter, ultracool dwarfs (UCDs)) have proved fruitful (e.g., Berger et al. 2001; Berger 2002; Hallinan et al. 2007; McLean et al. 2012; Route & Wolszczan 2012, 2016; Kao et al. 2016). Over two dozen brown dwarfs with spectral types L and T have been detected in the radio (Berger 2002; McLean et al. 2012; Williams 2018; Kao & Sebastian Pineda 2022). The detection of emission from the T2.5 dwarf SIMP J01365663+0933473 ($M = 12.7 \pm 1.0\, M_J$) established that even planetary-mass objects can emit at GHz frequencies (Kao et al. 2018). Unlike the magnetic field of a star like our Sun, which is generated by shear in the tachocline (Parker 1955), the dynamos of UCDs are thought to be convection generated, which is also the case for planets in our solar system (Christensen et al. 2009). This dynamo process was initially predicted to generate only weak magnetic fields, but this has now been refuted by the properties of the radio emission, which require kG-level large-scale fields (Berger 2002; Williams et al. 2014; Hallinan et al. 2015). In fact, recent results have shown spatially resolved emission around the UCD LSR J1835+3259, which potentially indicates the presence of a planet-like radiation belt (Climent et al. 2023; Kao et al. 2023), suggesting that the strong magnetic fields in UCDs may be "planet-like" in nature (Williams 2018). The detection of GHz frequency radio emission from UCDs thus implies that exoplanets may also be capable of generating strong enough magnetic fields to cause detectable radio emission at these frequencies, where sensitive searches can be carried out. This serves as the main motivation for this work.

In Cendes et al. (2021), we conducted a pilot search for GHz frequency emission from a small sample of five systems with eight exoplanets, which had all been discovered via direct imaging. Directly imaged exoplanets are an attractive sample due to their comparable mass scale to T dwarfs and due to their resolvable angular separation from their host stars in the VLA observations. Furthermore, these planets are generally younger and warmer and thus expected to have stronger convection and a more active dynamo (Reiners & Christensen 2010). Our pilot study did not detect any of these targets but established luminosity upper limits of $\lesssim 10^{12.5}$ erg s^{-1} Hz^{-1}, comparable to the detected emission from some T dwarfs (Pineda et al. 2017).

The number of nearby directly imaged exoplanets is currently small, especially in the context of radio detection rates of UCDs of ∼5%–10% (Berger 2002; McLean et al. 2012; Route & Wolszczan 2016). To achieve statistically meaningful results that could constrain the presence of radio emission from exoplanet systems requires a much larger sample of nearby systems. Such a sample will also naturally span a wide range of masses, thereby exploring radio emission from Earth-mass to multi-Jupiter-mass systems. Here, we present the results of the first large-scale GHz frequency survey of nearby exoplanet systems, predominantly within 17.5 pc using the Very Large Array (VLA), combining new data with archival observations. In Section 2 we present the survey and experimental design. In Section 3 we present the results of the observations, and in Section 4 we discuss their implications; we end with concluding remarks in Section 5.

2. Sample Selection and Observations

We constructed a target sample using the NASA Exoplanet Archive,[3] which included about 5500 confirmed exoplanets at the time of the sample construction in early 2023. We imposed the following selection criteria: (i) companion mass of $<13\, M_J$ to ensure exoplanet targets; (ii) distance of <17.5 pc to ensure that we can reach luminosity limits of about $10^{12.5}$ erg s^{-1} Hz^{-1}, comparable to the faintest UCDs, in a reasonable amount of observing time; and (iii) decl. of $> -25°$ for accessibility and ease of scheduling with the VLA. This led to a complete, volume-limited target sample of 83 targets containing 145 exoplanets. Of these targets, we were awarded sufficient observing time for observations of 56 targets.[4] We further supplemented these observations with analysis of archival data for an additional 9 targets that meet our selection criteria. In total, we present results for 65 of the 83 targets in this first target sample. In addition, we also include in our survey 2 targets below our decl. cutoff, and 10 targets slightly outside our distance cutoff for a total of 77 targets studied in this work. A summary of the number of targets observed and the number of targets used in the results of this study is provided in Table 1.

2.1. New VLA Observations

We obtained observations with the VLA as part of programs 22A-186 (PI: Cendes) and 23A-270 (PI: Ortiz Ceballos); details are shown in Table 1. All observations were performed in the *C* band, with continuous spectral coverage at 4–8 GHz. We selected *C* band due to its optimal sensitivity and since UCD radio emission has been predominantly detected at this frequency range (e.g., Berger et al. 2005, 2009; Williams et al. 2013; Kao et al. 2016, 2018). We selected observing times proportional to the distance to each target to achieve a luminosity limit of $\approx 10^{12.5}$ erg s^{-1} Hz^{-1} or better across the sample.

[3] https://exoplanetarchive.ipac.caltech.edu/

[4] One additional target, 61 Vir, was also observed in our programs, but its location was contaminated by bright emission from a nearby source; we therefore consider it an unobserved target.

Table 1
VLA Programs Used in this Study

Program ID	Dates Observed	Configurations	Targets Observed	Targets Used
22A-186	2022-03-01 to 2022-07-02	A, BnA → A	37	35
23A-270	2023-03-29 to 2023-05-14	B	23	23
15B-326	2015-11-17 to 2016-01-21	D, DnC	21	5
18B-048	2019-01-14 to 2019-02-16	C, C → B	27[a]	14

Note.
[a] The number of targets observed in *C* band for this program.

2.2. Archival Data

We additionally identified unpublished data in the VLA archive that include exoplanets within our 17.5 pc cutoff (or close to it). These programs are listed in Table 1, along with their observational details. For program 18B-048 (PI: Bastian), we only used observations in *C* band to match our own data. In the case of both archival programs, we also excluded targets that we already observed as part of our new programs, given our greater sensitivity.

2.3. Data Analysis

For programs 18B-048, 22A-186, and 23A-080, the calibrated measurement sets were obtained from the National Radio Astronomy Observatory (NRAO) archive, having been processed by the Common Astronomy Software Application package (CASA; McMullin et al. 2007) standard 6.4.1 pipeline. In the case of program 15B-326 (PI: Bastian), the calibration files were separately obtained from the NRAO archive and used to calibrate the raw visibilities with CASA 4.3.1.

Images for each target were made using the standard `CLEAN` algorithm with the CASA `tclean` procedure, with a pixel size of 1/3 of the synthesized beam size for each observation. We then obtained Gaia DR3 coordinates and proper motions for each target, which have submilliarcsecond and submilliarcsecond/year precision, respectively, for all targets in our sample (Gaia Collaboration et al. 2016, 2023). We generated proper-motion-corrected coordinates for the time of observation for each target.

We used these coordinates to perform point-source photometry on the images at the location of the targets using the `imtool fitsrc` feature of `pwkit` (Williams et al. 2017). Of the 77 targets, only 1 resulted in a $>5\sigma$ detection of a point source. The resulting flux densities were scaled to spectral luminosities using the distances from the Gaia parallaxes. Results are tabulated in Tables 2, 3, 4, and 5.

3. Results

We obtained 1 detection and 76 nondetections from the 77 systems, containing 140 exoplanets. The results are shown in Figure 1, where we plot luminosities as a function of distance. At $\lesssim$8 pc, our luminosity upper limits are $\approx 10^{11}$–10^{12} erg s^{-1} Hz^{-1}, and they reach our nominal target limit of $\approx 10^{12.5}$ erg s^{-1} Hz^{-1} to $\approx$17.5 pc; the limits beyond 17.5 pc (from archival data) are shallower by about 0.5 dex. Our detection of GJ 3323 is at a level of $\approx 10^{12.5}$ erg s^{-1} Hz^{-1}, and we discuss this in more detail in Section 3.1. These results are consistent with previous searches for radio emission from exoplanet systems at GHz frequencies (e.g., Bastian et al. 2000; Route 2019; Cendes et al. 2021), which have found no emission from similar targets, although with much smaller sample sizes.

In Figures 2 and 3 we show the same luminosity limits but now for each exoplanet with respect to their mass and orbital separation, respectively. Our survey probes a wide planetary-mass range of $\approx 10^{-3}$–$10\,M_J$. We also compare our results with a few existing measurements of low-mass UCDs for which quiescent radio emission is detected and a mass estimate is available. Unlike planets, for which masses can be measured from their orbital motion, these low-mass stars require comparing observed spectra with atmospheric evolution models to estimate the object's mass. Finally, Figure 3 shows that we probe orbital separations from 10^{-2} to 10^{1} au.

In all three figures we also present a few existing observations from the literature from comparable 4–8 GHz observations. Pineda & Hallinan (2018) found a limit of $<1.43 \times 10^{12}$ erg s^{-1} Hz^{-1} from 4 to 8 GHz observations on TRAPPIST-1. Bower et al. (2009) found a limit of $<6.5 \times 10^{12}$ erg s^{-1} Hz^{-1} for GJ 625 as part of a survey of stars. Bastian et al. (2018) detected ϵ Eridani at $(1.0 \pm 0.2) \times 10^{12}$ erg s^{-1} Hz^{-1} but concluded that the detection is likely of stellar origin. We also included the result for the one target in our pilot study (Cendes et al. 2021) that falls within our distance cutoff, Ross 458. That study found a limit of $<1.4 \times 10^{12}$ erg s^{-1} Hz^{-1}. Unlike the limits presented in this work, that limit constrains emission from the planet directly since the planet was resolvable in the observation. All of these measurements were taken with the VLA.

Given the individual nondetections, we generated stacked images for each observing program with a sufficient number of targets (i.e., 18B-048, 22A-186, and 23A-270) by aligning the individual images centered on the known position of each source; we stacked the images in this manner given the different VLA array configurations (and hence angular resolution) of each program. In the 22A-186 stack we excluded GJ 3323 given its individual detection. The stacked images are shown in Figure 4 and do not reveal any significant emission at the source locations. The resulting rms noise levels are 2.1, 1.1, and 1.0 μJy for the 18B-048, 22A-186, and 23A-270 stacks, respectively. Collectively, this indicates that any steady emission from exoplanets at this frequency range has a typical flux density of $\lesssim$1–2 μJy.

3.1. Detection of GJ 3323

Our single detection from the survey is of the GJ 3323 system (5.37 pc), which consists of an M4 star with two terrestrial planets, GJ 3323 b ($M_p \sin i = 2.02 M_\oplus$, $P = 5.36$ days) and GJ 3323 c ($M_p \sin i = 2.31 M_\oplus$, $P = 40.54$ days; Astudillo-Defru et al. 2017). GJ 3323 has been previously detected with the Chandra X-ray Observatory with a luminosity of $\log L_X = 27.28$ erg s^{-1}

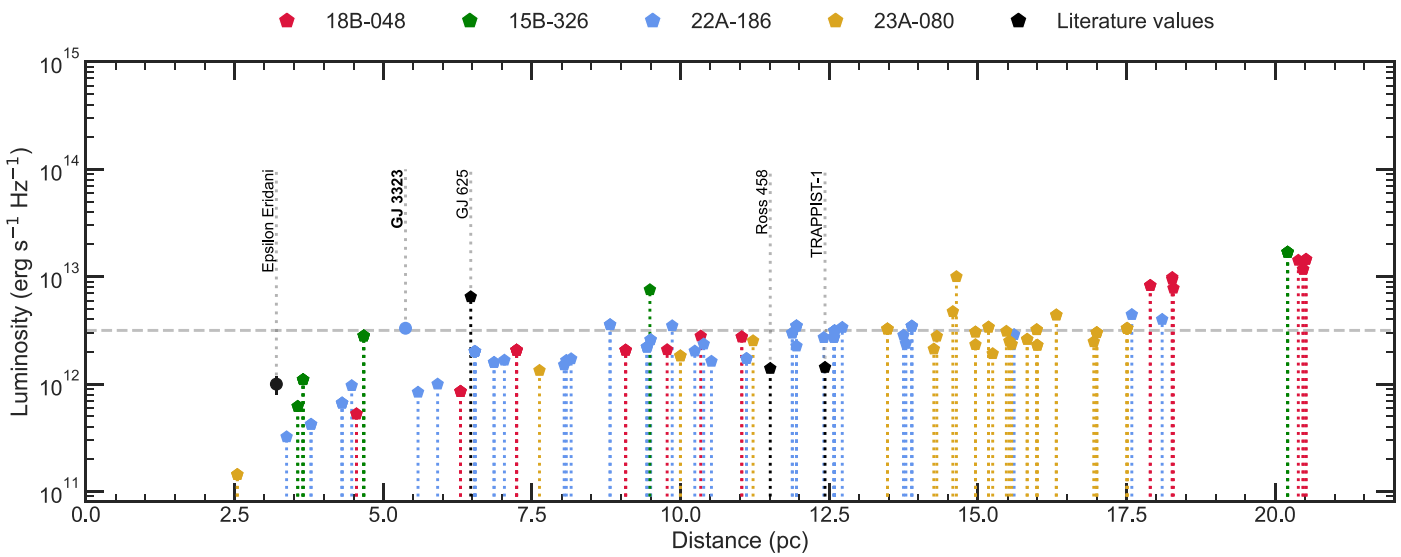

Figure 1. Luminosity upper limits as a function of system distance. A dashed line shows the intended sensitivity of the survey at $L_\nu \lesssim 10^{12.5}$ erg s^{-1} Hz^{-1}. Each data set studied is shown in a different color, and upper limits on luminosity as a function of distance are presented as markers with dotted lines pointing downward. Results from the literature are also shown for reference; these correspond to the four systems in the unobserved portion of the sample that have published radio observations in the 4–8 GHz range, taken from Bower et al. (2009), Bastian et al. (2018), Pineda & Hallinan (2018), and Cendes et al. (2021).

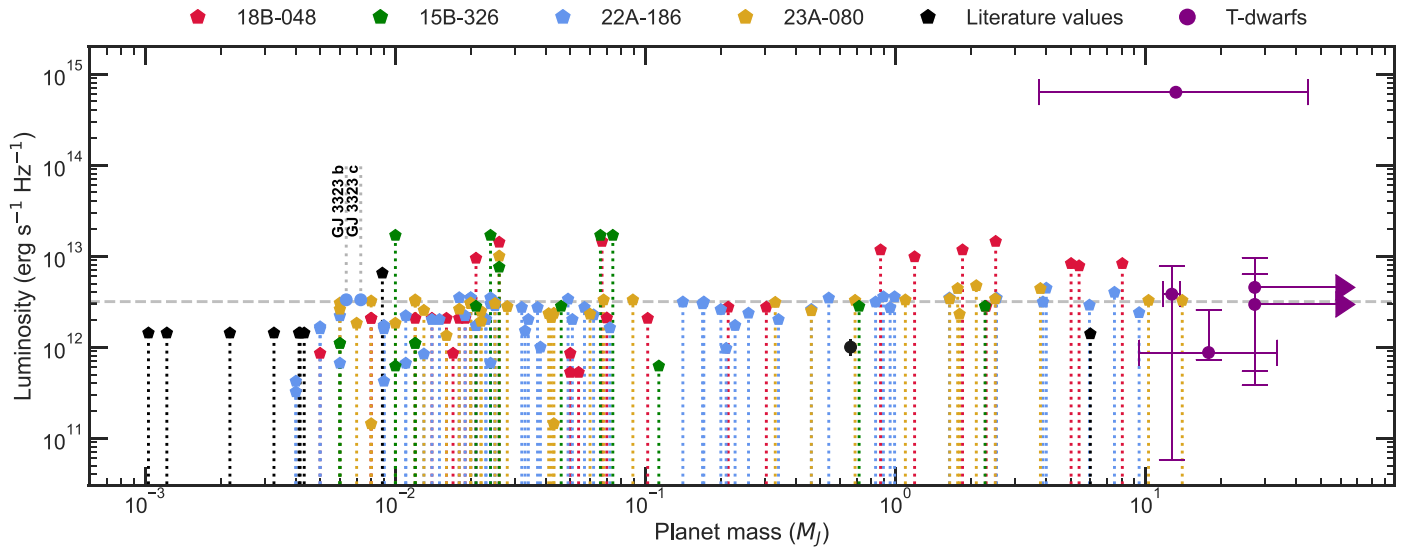

Figure 2. Luminosity limits as a function of planet mass. Here, each planet in the sample is plotted, with the luminosity measurement corresponding to its system. We include the same four literature systems as in Figure 1. We also include the measured luminosities and estimated masses for the available radio-detected T dwarfs in the literature: SIMP J013656.5+093347.3, 2MASS J10475385+2124234, 2MASS J12373919+6526148, 2MASS J12545393-0122474, and WISE J062309.94-045624.6. These literature measurements are taken from Kao et al. (2016, 2018) and Rose et al. (2023).

(0.5–8 keV) and with ROSAT with a luminosity of $\log L_X = 27.45$ erg s^{-1} (0.1–2.4 keV; Wright et al. 2018). Furthermore, we identify the source in the SRG/eROSITA all-sky survey Data Release 1 (Merloni et al. 2024) with a luminosity of $\log L_X = 27.32$ erg s^{-1} (0.2–2.3 keV). GJ 3323 has an estimated Rossby number of 0.87 that places it in the "unsaturated" regime of the rotation–activity relation (Boudreaux et al. 2022).

In our VLA observation, we detect GJ 3323 with a flux density of 86 ± 10 μJy, corresponding to a luminosity of $\log(L_\nu) = 12.47 \pm 0.05$ erg s^{-1} Hz^{-1}. We also detect it in Stokes V (circular polarization) with a flux density of 35 ± 9 μJy, corresponding to a circular polarization fraction of $\approx$40%. The VLA detection is shown in Figure 5, with the total intensity (Stokes I) in the top panel and the circular polarization (Stokes V) in the bottom panel. We estimate a spectral index of $\alpha = 1.0^{+0.7}_{-0.9}$ in the observed 4–8 GHz range, although the large uncertainty and narrow spectral range make the inference of spectral shape inconclusive.

Using the radio and X-ray luminosities, we can compare the results for GJ 3323 to the Güdel–Benz Relation (GBR; Guedel & Benz 1993; Benz & Guedel 1994), an empirical power-law relation between the radio and X-ray luminosities of active stars. Stars of spectral types earlier than M7 typically closely follow this relation, spanning almost 10 orders of magnitude in radio and X-ray luminosities (Williams 2018).

We find that GJ 3323 is located close the GBR, indicating that the radio emission is consistent with having a stellar origin. Our GJ 3323 detection places it 0.57 dex perpendicular from the GBR best-fit line, while the perpendicular scatter of the original Güdel–Benz sample is 0.2 dex (Williams et al. 2014). However, stars of

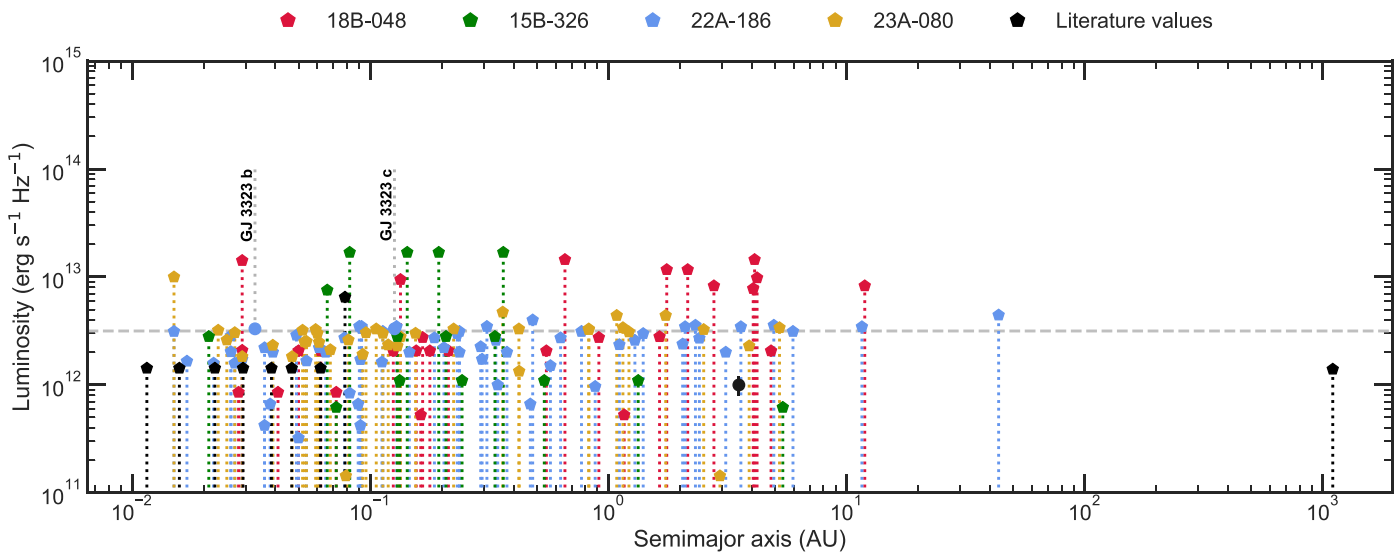

Figure 3. Luminosity limits as a function of planet orbital separation. The literature values correspond to the same four systems from Figures 1 and 2.

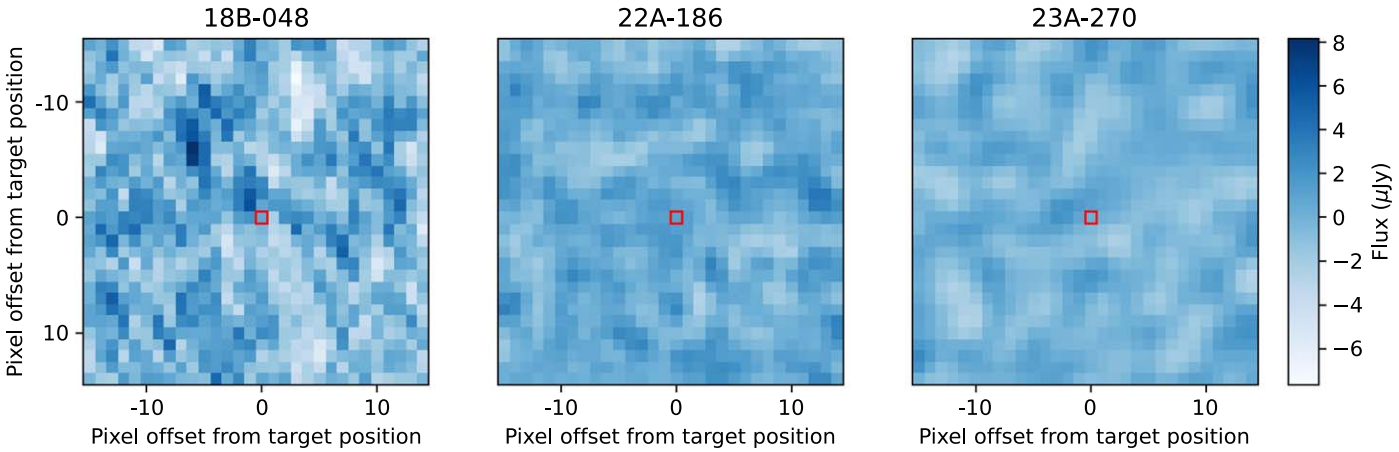

Figure 4. Stacked images for targets from three of the VLA programs reported in this paper. Each stack is made using a weighted average of a 31 x 31 pixel region centered on each target star. The center pixel is marked with a red outline. Images were made with a cell size of 1/3 the synthesized beam size, but there may be more than one beamwidth per stack. The resulting rms values for the stacks are 2.1 μJy (18B-048), 1.1 μJy (22A-186), and 1.0 μJy (23A-270).

spectral type M0–M6 with radio and X-ray detections tend to skew to the left of the GBR fit (Williams et al. 2014), and GJ 3323 is not exceptional in this (see the inset of Figure 6).

It is important to note that M dwarf X-ray and radio emission can show flaring and variability on a timescale of minutes to hours (e.g., Berger 2002; Stelzer et al. 2006; Antonova et al. 2007), such that relying on nonsimultaneous observations for placing targets in the GBR can be risky. However, the consistent X-ray luminosity from Chandra, ROSAT, and eROSITA suggests that the X-ray emission is quiescent in nature. For our radio observation, the light curve did not vary over the 11 minutes duration, but the short observation time makes further characterization difficult. We also checked VLA Sky Survey (Lacy et al. 2020) epochs 1, 2, and 3 for emission from the proper-motion-corrected location of GJ 3323 but did not detect a source (to shallow 3σ limits of $\approx$0.40 mJy at 3 GHz).

Despite the overall consistency with a stellar emission origin, the relatively high circular polarization fraction could point to a planetary origin, which we discuss in more detail in Section 4.

4. Discussion

The possibility of radio emission from exoplanet systems has been discussed in the literature in the context of three possible processes: star–planet interaction, direct planetary emission, or stellar emission. We discuss each of these scenarios in the following.

4.1. Star–Planet Interaction

In the solar system, the strength of radio emission from magnetized planets (the radio power output) is directly proportional to the electromagnetic Poynting flux incident on the magnetopause of the planet due to the solar wind, a relation known as the radiometric Bode's law (RBL; Desch & Kaiser 1984). Historically, the RBL has been used as a scaling law to predict the strength of putative radio emission from exoplanets from their estimated magnetic fields (Lazio et al. 2004; Zarka 2007). However, the RBL is an empirical relation determined only from planets orbiting the same star, our Sun. Given the dependence of this behavior on the solar wind, it is

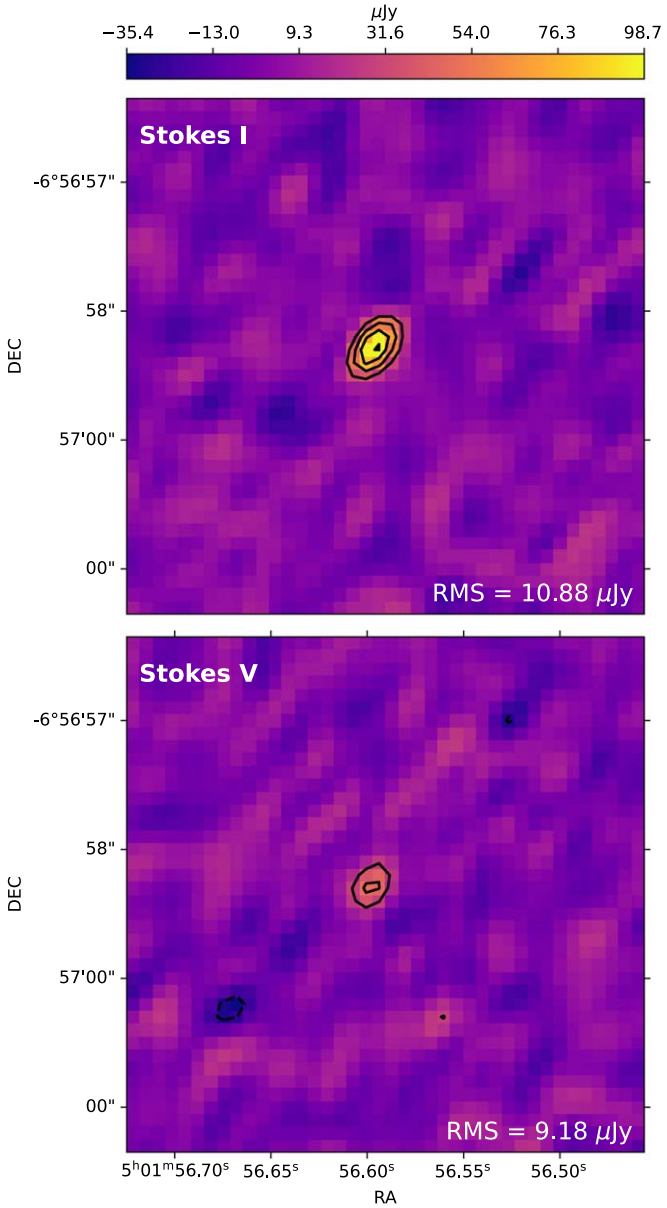

Figure 5. VLA images of the region centered on the Gaia DR3 proper-motion-corrected position of GJ 3323. The contour levels are -3, 3, 5, 7, 9σ, where σ is the rms of the image as shown in each cutout. GJ 3323 is detected with a flux density of 86 ± 10 μJy in Stokes I and 35 ± 9 μJy in Stokes V.

risky to extrapolate this to other stellar systems, especially to systems with stars much different than the Sun.

In the case of M dwarfs, it becomes particularly necessary to take into account that these stars are known to be significantly more active and have distinct environments from Sun-like stars. Many of these systems also have close-in exoplanets, which have been proposed to be ideal targets for searching for exoplanet-induced radio emission due to increased possibility of observable star–planet interaction stemming from these short orbital separations (Cuntz et al. 2000). Planets in close orbits around their stars are immersed in flowing magnetized plasma from the stellar environment. The planets themselves thus become obstacles to the plasma flow and interact with it, causing waves in this flow. In sub-Alfvénic modes, energy gets transported back to the star and can also be observed as radio emission (Saur et al. 2013). No solar system planets have this kind of interaction with the Sun, owing to their large orbital

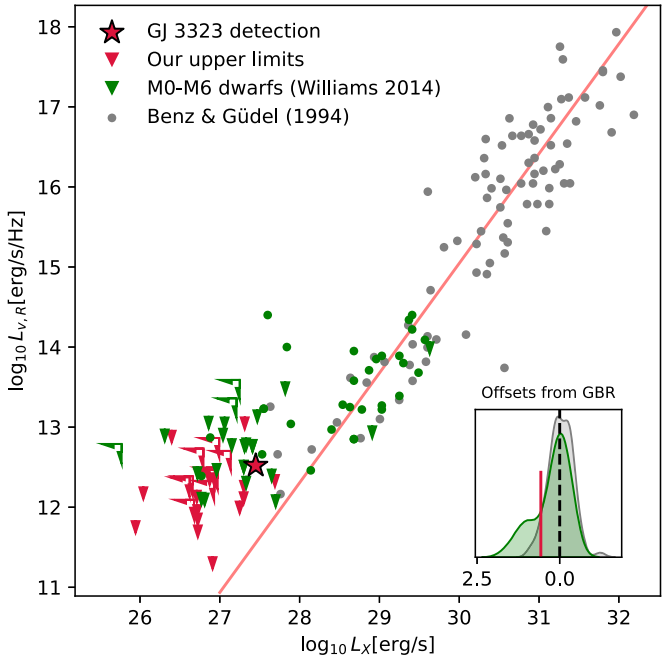

Figure 6. The GBR between X-ray and radio luminosities. The red arrows indicate upper limits on GBR placement obtained from our radio luminosity upper limits and X-ray luminosity values from Stelzer et al. (2013). The red star indicates the placement of GJ 3323 in the GBR from our detection. Gray circles are from the original result of Benz & Guedel (1994), and green circles and arrows are detections and upper limits, respectively, of early M dwarfs (M0–M6) from Williams et al. (2014). The inset plot shows the distribution of offsets perpendicular to the GBR fit in units of dex for the original Güdel–Benz sample (gray) and for the Williams et al. (2014) sample (green), with GJ 3323 as the red line.

distances; sub-Alfvénic interaction is responsible for the observed "Jupiter–Io" effect in which periodic radio emission and auroral activity are observed in phase with the orbit of Io (Zarka 2007), but this is due to magnetospheric currents generated by Jupiter's rotation instead of a wind.

Sub-Alfvénic interaction, however, could be the case in the GJ 3323 system. GJ 3323 b has been estimated to be within the Alfvén surface radius of its host star (with GJ 3323 c just outside the radius), raising the possibility of star–planet interaction as a driver of radio emission (Farrish et al. 2019), even though comparison with Alfvén wave models of the similarly slowly rotating Proxima Centauri is not as optimistic (Kavanagh et al. 2021). The radio emission observed from the Jupiter–Io system is coherent and nonthermal, caused by ECMI (Zarka 2007). In this mechanism, the observed frequency of emission (the cyclotron frequency ν_c) is proportional to a magnetic field strength and provides a "point estimate" of this field strength (B) at the point of emission in the object where the cyclotron maser occurs. This means that the field does not need to be this strong everywhere, or even on average, but just somewhere in the system. The cyclotron frequency is given by:

$$\nu_c = \frac{eB}{2\pi m_e c} \approx 2.8\left(\frac{B}{1\ \mathrm{kG}}\right)\ \mathrm{GHz}. \quad (1)$$

ECMI emission exhibits a sharp drop-off in flux at frequencies higher than the cyclotron frequency, such that the mere detection of ECMI diagnoses the cyclotron frequency and thus the magnetic field strength. For our frequency range of 4–8 GHz, the above equation yields magnetic field strengths of 1.4–2.8 kG. It should be noted that the time dependence of

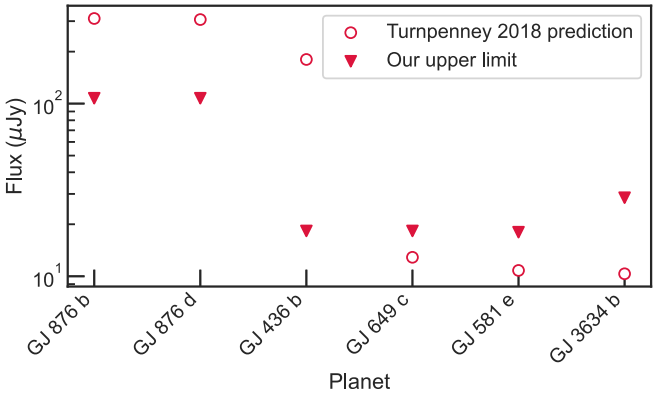

Figure 7. Flux predictions from Turnpenney et al. (2018) for six nearby exoplanets and our measured upper limits. We establish upper limits more stringent than their predicted fluxes for three planets. Two of these planets belong to the same system, GJ 876.

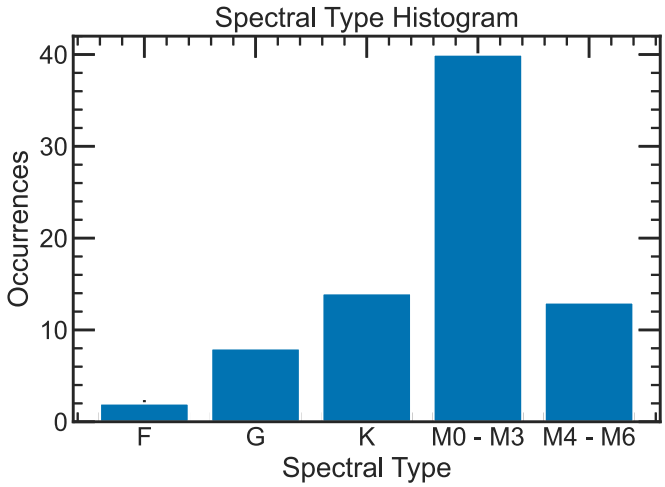

Figure 8. Spectral-type distribution of our observed sample of stellar systems. The spectral type for each observed star is taken from the NASA Exoplanet Archive's Planetary Systems Composite Planet Data Table.

ECMI bursts, as well as significant beaming effects that occur in the ECMI emission, introduce additional challenges toward detecting this kind of emission with short observations like ours (Zarka 2007).

ECMI emission is typically characterized by a high circular polarization fraction (Treumann 2006). The circular polarization fraction of 40% we detect from GJ 3323 is unfortunately ambiguous and, especially at GHz frequencies, insufficient to identify the observed emission as caused by ECMI (Villadsen & Hallinan 2019). Furthermore, the brief observation presented here cannot truly check for or rule out star–planet interaction since, as a single snapshot, it cannot be correlated with the planets' orbital periods.

Beyond the detection of GJ 3323, we also investigate our upper limits in comparison with existing predictions. Turnpenney et al. (2018) examined the closest M dwarf systems with close-in planets and modeled this behavior to predict their radio fluxes. In Figure 7, we show the predicted fluxes for these systems in comparison to our observed limits. We observed 6 of the 11 exoplanets identified by Turnpenney et al. (2018) as the strongest likely emitters. For 3 of these planets, our observations establish upper limits that are between 3 and 10 times fainter than the predicted flux. For the remaining 3, our limits are about a factor of 2 times higher than the predicted flux.

It is important to note that these predictions involve poorly constrained assumptions about the planetary and stellar magnetic field strengths of the systems in question and the stellar wind mass outflow rates. Furthermore, the ECMI emission that is considered in this model is taken to have a flat spectral profile up to an unspecified cutoff frequency in the GHz range at which the brightness declines rapidly. The cutoff frequency is proportional to the stellar magnetic field strength in the region of emission. While global magnetic fields for M dwarfs can often reach a few kG (Reiners et al. 2009), what matters for ECMI emission is the magnetic field strength at the location of emission. Notably, it can plausibly reach the 2−4 kG threshold probed by our 4–8 GHz observations even in stars with low global field strength (Pineda & Hallinan 2018).

Observations of coherent emission at 1.6 GHz from Proxima Centauri have been found to coincide with the orbital period of its innermost planet, suggesting that the emission is caused by star–planet interaction (Pérez-Torres et al. 2021). Pineda & Villadsen (2023) published a detection of coherent emission from the YZ Ceti system at 2–4 GHz using the VLA. Two bursts of emission were detected, and they coincided with the same moment of orbital phase of the only planet in the system, YZ Ceti b, which has a 2 day period orbit. Trigilio et al. (2023) independently observed emission in the 0.55–0.9 GHz band, using the Giant Metrewave Radio Telescope, also in phase with the planetary orbit. This is tentative evidence that the bursts may be caused by star–planet interaction. In this case, the actual emission may be coming from the star itself, similar to the observed Jupiter–Io effect in the solar system.

We note that for the observed bursts for both Proxima Centauri and YZ Ceti, these could last from minutes to hours. If these signals are in fact the result of star–planet interaction, their occurrence will depend on the planetary orbital period. Given their short duration with respect to a full orbit, then the nondetections presented in this work do not rule out that any of our targets may exhibit these interactions. The bursts observed from YZ Ceti peaked at a luminosity of $L_\nu \sim 10^{13}$ erg s^{-1} Hz^{-1}, within the sensitivity of our survey.

4.2. Direct Emission from Exoplanets

Beyond emission from star–planet interactions, it is also important to consider direct planetary radio emission. In principle, ECMI emission could be produced and detected directly from an exoplanet. As mentioned previously, if emission were caused by ECMI, a detection at our observed frequencies would correspond to a kilogauss magnetic field; this is beyond the estimated planetary magnetic field strengths of even the largest exoplanets. However, low-mass UCDs were long predicted to have weak magnetic fields (Durney et al. 1993; Mohanty et al. 2002) before the detection of their bright radio emission. In UCDs, ECMI emission is observed in flares that can be detected even when the object does not exhibit steady quiescent emission (Berger 2002; Route & Wolszczan 2016). Furthermore, since the observed cyclotron frequency is proportional to a magnetic field "point estimate," the field does not need to be as strong everywhere, or even on average, but just somewhere in the system at a time of observation.

While convected energy scaling laws suggest that even super-Jupiter exoplanets would exhibit much lower ECMI cyclotron frequencies than the GHz range, the observed UCD emission suggests these scaling laws may not be valid for all planetary-mass objects (Christensen et al. 2009; Kao et al.

2018). On the other hand, models suggest that young or more massive planets could have field strengths as strong as ∼0.1 kG (Hori 2021); this is still not enough for direct ECMI emission from these planets to be detectable at GHz frequencies.

In addition to the field strength, a population of nonthermal electrons is also required in the planetary environment so that ECMI can take place. These electrons could be provided by the stellar wind or perhaps by satellites of the planet, as occurs in the Jupiter system (Noyola et al. 2014, 2016). Finally, the challenges of the beaming and time dependence of ECMI bursts mentioned previously also apply, making the prospect of detecting direct emission even more uncertain.

An alternative direct emission mechanism could be gyrosynchrotron emission, which is also present in UCDs in the form of stable, quiescent emission. This type of emission is caused by mildly relativistic electrons moving in a stellar/planetary magnetic field (Williams 2018). Stellar activity could further exacerbate these electrons into producing synchrotron bursts directly in the planetary environment, but this behavior has not yet been observed (Gao et al. 2020). Like with ECMI, both a strong magnetic field and nonthermal electrons are required to be present. While gyrosynchrotron emission can be present at much higher frequencies for a given magnetic field strength compared to ECMI (such that in principle GHz observations could probe weaker magnetic fields than with ECMI observations), as an incoherent mechanism it is also much less efficient and is expected to be around 5 orders of magnitude weaker (Zarka et al. 2015) beyond what can be probed with the sensitivity of the VLA.

4.3. Stellar Radio Emission

While target selection for our survey was motivated by the known presence of exoplanets, our results are also relevant to the broader study of stellar radio emission. Our target stars span the F, G, K, and M spectral types, with the specific breakdown of spectral types shown in Figure 8.

Notably, we did not observe any UCDs (spectral types $\gtrsim$M7); the only two UCDs that meet our survey selection criteria for companion mass, system distance, and target decl. are TRAPPIST-1 and Teegarden's Star. TRAPPIST-1 has a published luminosity upper limit of $\log_{10}(L_\nu) = 12.15\,\mathrm{erg\,s^{-1}\,Hz^{-1}}$ from a 4–8 GHz observation with the VLA (Pineda & Hallinan 2018). UCDs can be significantly bright in the radio, several orders of magnitude brighter than the GBR would predict (Williams et al. 2014). Meanwhile, earlier-type M dwarfs are generally fainter in the radio with respect to their bolometric luminosity and less likely to be detected at all (Berger 2006).

In our survey, we observed a total of 53 M dwarfs, comprising 40 early-M dwarfs (spectral type M0–M3) and 13 mid-M dwarfs (M4–M6). Out of these 53 observations, we only detected one star, GJ 3323. Given the large number of M dwarfs observed, our results are relevant to recent searches for radio activity from these stars (e.g., Callingham et al. 2021). It is difficult to gauge the consistency of this survey's results with previous GHz observations of main-sequence stars given differences in sample selection. Bower et al. (2009) surveyed 172 active M dwarfs with the VLA at 5 GHz and detected 29; their survey sample was built from stars known to be active, for the purpose of identifying bright targets for astrometric study. Our results are more consistent with those of McLean et al. (2012), who observed 25 early-M dwarfs (M4–M6.5) within 20 pc, detecting only 1. However, a systematic study that does not select for activity (or as in our case, the presence of known exoplanets) is necessary to make more definitive conclusions on the radio brightness of these stars.

5. Conclusions

We have presented VLA radio observations at 4–8 GHz of 77 nearby exoplanet systems, reaching a luminosity sensitivity limit of $\approx 10^{12.5}\,\mathrm{erg\,s^{-1}\,Hz^{-1}}$. This sensitivity limit is comparable to our previous pilot study (Cendes et al. 2021) and to detections of radio emission from UCDs (e.g., Berger 2002; McLean et al. 2012) and is more sensitive than previous searches for exoplanet radio emission at GHz frequencies (e.g., Bastian et al. 2000). We detect a single target, GJ 3323 (M4) with a spectral luminosity of $\log(L_\nu) \approx 12.5\,\mathrm{erg\,s^{-1}\,Hz^{-1}}$. Comparing this result to the known X-ray luminosity of this source suggests that the emission is likely of stellar origin, but the relatively high fraction of circular polarization may be indicative of star–planet interaction.

Due to the nature of our survey, the observing time was optimized toward reaching a desired sensitivity for a large number of targets. Bursty or intermittent emission may have well been missed in our short observations, and although our large number of targets mitigates this limitation in the aggregate, any individual system observed may still be an intermittent emitter. Future long-term monitoring of dedicated targets may detect intermittent emission and may be able to characterize it as of planetary origin through correlation with the planetary orbital period.

Future searches for exoplanet radio emission in the GHz regime may have the capacity to go beyond what has been done in this work thanks to the advent of more sensitive radio telescopes in the next decade, such as the Next-Generation Very Large Array (ngVLA) and the Square Kilometre Array (SKA; Selina et al. 2018; Braun et al. 2019). It is estimated that SKA1 will achieve an order of magnitude improvement in sensitivity over the VLA for observations of stellar sources, with sensitivity as low as $\sim 2\,\mu$Jy for 1 hr integrations. SKA2 and ngVLA will improve another order of magnitude to $\sim 0.2\,\mu$Jy (Pope et al. 2019). With these capabilities, it may be possible to either detect or rule out the more optimistic predictions for the brightness of radio emission due to star–planet interactions (Turnpenney et al. 2018).

Acknowledgments

We thank Tim Bastian, Robert Kavanagh, and Joe Callingham for useful discussions. The Berger Time-Domain Group at Harvard is supported by NSF and NASA grants; this work was supported by NSF grant AST-2007411. The National Radio Astronomy Observatory is a facility of the National Science Foundation operated under cooperative agreement by Associated Universities, Inc. This research has made use of the NASA Exoplanet Archive, which is operated by the California Institute of Technology, under contract with the National Aeronautics and Space Administration under the Exoplanet Exploration Program. We also appreciate the support from the NSF Graduate Research Fellowship (GRFP), grant No. DGE1745303, and of the Ford Foundation Predoctoral Fellowship. This work has made use of data from the European Space Agency (ESA) mission Gaia (https://www.cosmos.esa.int/gaia), processed by the Gaia Data Processing and Analysis

Consortium (DPAC; https://www.cosmos.esa.int/web/gaia/dpac/consortium). Funding for the DPAC has been provided by national institutions, in particular the institutions participating in the Gaia Multilateral Agreement.

Appendix

In Tables 2–5, we list the complete results of the survey for all four VLA programs analyzed.

Table 2
15B-326 Results

Target System	Distance (pc)	Planet	Planet Mass (M_J)	Semimajor Axis (au)	rms (μJy)	Luminosity (erg s^{-1} Hz^{-1})
Gl 15A	3.562	b	0.010	0.072	13.6	$<6.20 \times 10^{11}$
...	...	c	0.113	5.400	...	...
τ Cet	3.652	e	0.012	0.538	23.0	$<1.10 \times 10^{12}$
...	...	f	0.012	1.334	...	...
...	...	g	0.006	0.133	...	...
...	...	h	0.006	0.243	...	...
Gl 876	4.672	b	2.276	0.208	35.8	$<2.81 \times 10^{12}$
...	...	c	0.714	0.130	...	...
...	...	d	0.021	0.021	...	...
...	...	e	0.046	0.334	...	...
GJ 176	9.485	b	0.026	0.066	23.4	$<7.56 \times 10^{12}$
GJ 3293	20.21	b	0.074	0.143	11.5	$<1.69 \times 10^{13}$
...	...	c	0.066	0.362	...	...
...	...	d	0.024	0.194	...	...
...	...	e	0.010	0.082	...	...

Note. Luminosities determined from three-times-measured rms (3σ) and distance.

Table 3
18B-048 Results

Target System	Distance (pc)	Planet	Planet Mass (M_J)	Semimajor Axis (au)	rms (μJy)	Luminosity (erg s^{-1} Hz^{-1})
Gl 687	4.55	b	0.054	0.163	7.1	$<5.28 \times 10^{11}$
...	...	c	0.050	1.165	...	...
Gl 581	6.3	b	0.050	0.041	6.0	$<8.55 \times 10^{11}$
...	...	c	0.017	0.072	...	...
...	...	e	0.005	0.028	...	...
Gl 667C	7.243	b	0.018	0.050	11.0	$<2.07 \times 10^{12}$
...	...	c	0.012	0.125	...	...
...	...	e	0.008	0.213	...	...
...	...	f	0.008	0.156	...	...
...	...	g	0.014	0.549	...	...
Gl 433	9.077	b	0.019	0.062	7.0	$<2.07 \times 10^{12}$
...	...	c	0.102	4.819	...	...
...	...	d	0.016	0.178	...	...
Gl 436	9.775	b	0.070	0.029	6.1	$<2.09 \times 10^{12}$
Pollux[a]	10.34	b	2.300	1.640	7.3	$<2.80 \times 10^{12}$
HIP 57050	11.03	b	0.304	0.166	6.3	$<2.75 \times 10^{12}$
...	...	c	0.214	0.912	...	...
14 Her	17.9	b	8.053	2.774	7.2	$<8.28 \times 10^{12}$
...	...	c	5.025	11.924	...	...
HD 154088	18.27	b	0.021	0.134	7.9	$<9.47 \times 10^{12}$
HD 154345	18.27	b	1.190	4.210	8.2	$<9.82 \times 10^{12}$
HD 87883	18.29	b	5.409	4.055	6.5	$<7.81 \times 10^{12}$
Gl 3634	20.39	b	0.026	0.029	9.5	$<1.42 \times 10^{13}$
7 CMa	20.47	b	1.850	1.758	7.8	$<1.17 \times 10^{13}$
...	...	c	0.870	2.153	...	...
Gl 328	20.52	b	2.510	4.110	9.6	$<1.45 \times 10^{13}$
...	...	c	0.067	0.657	...	...

Note.
[a] Target coordinates, proper motion, and distance taken from the Hipparcos catalog (van Leeuwen 2007) due to unavailability in Gaia.

Table 4
22A-186 Results

Target System	Distance (pc)	Planet	Planet Mass (M_J)	Semimajor Axis (AU)	rms (μJy)	Luminosity (erg s^{-1} Hz^{-1})
Ross 128	3.375	b	0.004	0.050	7.9	$<3.23 \times 10^{11}$
GJ 273	3.786	b	0.009	0.091	8.2	$<4.22 \times 10^{11}$
...	...	c	0.004	0.036	...	...
Wolf 1061	4.308	b	0.006	0.038	10.0	$<6.66 \times 10^{11}$
...	...	c	0.011	0.089	...	...
...	...	d	0.024	0.470	...	...
GJ 9066	4.47	c	0.210	0.880	13.5	$<9.68 \times 10^{11}$
GJ 3323	5.375	b	0.006	0.033	7.2	3.31×10^{11}
...	...	c	0.007	0.126	...	...
GJ 251	5.585	b	0.013	0.082	7.5	$<8.40 \times 10^{11}$
HD 180617	5.915	b	0.038	0.343	8.0	$<1.00 \times 10^{12}$
HD 219134	6.542	b	0.015	0.039	13.1	$<2.01 \times 10^{12}$
...	...	c	0.014	0.065	...	...
...	...	d	0.051	0.237	...	...
...	...	f	0.023	0.146	...	...
...	...	g	0.034	0.375	...	...
...	...	h	0.340	3.110	...	...
LTT 1445A[a]	6.864	b	0.009	0.022	9.4	$<1.59 \times 10^{12}$
...	...	c	0.005	0.027	...	...
GJ 393	7.038	b	0.005	0.054	9.4	$<1.67 \times 10^{12}$
GJ 1151	8.043	c	0.033	0.571	6.5	$<1.51 \times 10^{12}$
GJ 486	8.079	b	0.009	0.017	7.1	$<1.66 \times 10^{12}$
Gl 686	8.16	b	0.021	0.091	7.2	$<1.72 \times 10^{12}$
GJ 849	8.815	b	0.893	2.320	12.8	$<3.57 \times 10^{12}$
...	...	c	0.990	4.950	...	...
GJ 357	9.436	b	0.006	0.036	6.9	$<2.21 \times 10^{12}$
...	...	c	0.011	0.061	...	...
...	...	d	0.019	0.204	...	...
GJ 3512	9.497	b	0.460	0.337	8.0	$<2.59 \times 10^{12}$
...	...	c	0.200	1.292	...	...
Gl 49	9.86	b	0.018	0.090	10.0	$<3.49 \times 10^{12}$
GJ 1265	10.24	b	0.023	0.026	5.4	$<2.03 \times 10^{12}$
GJ 649	10.39	b	0.258	1.112	6.1	$<2.36 \times 10^{12}$
HIP 48714	10.52	b	0.072	0.112	4.1	$<1.63 \times 10^{12}$
GJ 740	11.11	b	0.009	0.029	3.9	$<1.73 \times 10^{12}$
HD 3651	11.11	b	0.228	0.295	3.9	$<1.73 \times 10^{12}$
GJ 414A	11.88	b	0.024	0.232	5.9	$<2.99 \times 10^{12}$
...	...	c	0.169	1.400	...	...
GJ 180	11.95	b	0.020	0.092	6.8	$<3.48 \times 10^{12}$
GJ 96	11.95	b	0.062	0.291	4.4	$<2.26 \times 10^{12}$
...	...	c	0.020	0.129	...	...
...	...	d	0.024	0.309	...	...
GJ 179	12.41	b	0.950	2.410	4.9	$<2.71 \times 10^{12}$
HD 69830	12.58	b	0.032	0.078	4.8	$<2.73 \times 10^{12}$
...	...	c	0.037	0.186	...	...
...	...	d	0.057	0.630	...	...
55 Cancri	12.59	b	0.831	0.113	5.5	$<3.13 \times 10^{12}$
...	...	c	0.171	0.237	...	...
...	...	d	3.878	5.957	...	...
...	...	e	0.025	0.015	...	...
...	...	f	0.141	0.771	...	...
HD 190007	12.72	b	0.049	0.092	5.8	$<3.37 \times 10^{12}$
GJ 3779	13.75	b	0.025	0.026	4.2	$<2.85 \times 10^{12}$
γ Cep	13.79	b	9.400	2.050	3.5	$<2.39 \times 10^{12}$
47 UMa	13.89	b	2.530	2.100	5.0	$<3.46 \times 10^{12}$
...	...	c	0.540	3.600	...	...
...	...	d	1.640	11.600	...	...
τ Boo	15.61	b	5.950	0.049	3.3	$<2.89 \times 10^{12}$
GJ 504	17.59	b	4.000	43.500	4.0	$<4.44 \times 10^{12}$
70 Vir	18.1	b	7.490	0.481	3.4	$<4.00 \times 10^{12}$

Note.
[a] Target coordinates, proper motion, and distance taken from the Hipparcos catalog (van Leeuwen 2007) due to unavailability in Gaia.

Table 5
23A-080 Results

Target System	Distance (pc)	Planet	Planet Mass (M_J)	Semimajor Axis (au)	rms (μJy)	Luminosity (erg s^{-1} Hz^{-1})
GJ 411	2.546	b	0.008	0.079	6.2	$<1.44 \times 10^{11}$
...	...	c	0.043	2.940	...	...
GJ 514	7.628	b	0.016	0.422	6.4	$<1.34 \times 10^{12}$
HD 260655	9.998	b	0.007	0.029	5.1	$<1.83 \times 10^{12}$
...	...	c	0.010	0.047	...	...
Ross 508	11.22	b	0.013	0.054	5.6	$<2.53 \times 10^{12}$
υ And	13.48	c	13.980	0.828	5.0	$<3.26 \times 10^{12}$
...	...	d	10.250	2.513	...	...
...	...	b	0.688	0.059	...	...
GJ 480	14.26	b	0.042	0.068	2.9	$<2.12 \times 10^{12}$
GJ 685	14.31	b	0.028	0.134	3.8	$<2.79 \times 10^{12}$
HIP 79431	14.58	b	2.100	0.360	6.2	$<4.73 \times 10^{12}$
GJ 1214	14.64	b	0.026	0.015	13.0	$<1.00 \times 10^{13}$
LHS 1140	14.96	b	0.020	0.096	3.8	$<3.05 \times 10^{12}$
Gl 378	14.96	b	0.041	0.039	2.9	$<2.33 \times 10^{12}$
...	...	c	0.006	0.027	...	...
GJ 317	15.18	c	1.644	5.230	4.1	$<3.39 \times 10^{12}$
...	...	b	2.500	1.151	...	...
HD 238090	15.25	b	0.022	0.093	2.3	$<1.92 \times 10^{12}$
TYC 2187-512-1	15.48	b	0.330	1.220	3.6	$<3.10 \times 10^{12}$
51 Peg	15.53	b	0.460	0.053	2.9	$<2.51 \times 10^{12}$
GJ 720A	15.57	b	0.043	0.119	2.7	$<2.35 \times 10^{12}$
GJ 3929	15.83	b	0.006	0.025	2.9	$<2.61 \times 10^{12}$
...	...	c	0.018	0.081	...	...
G 264-12	15.99	b	0.008	0.023	3.5	$<3.21 \times 10^{12}$
...	...	c	0.012	0.052	...	...
HD 190360	16.0	b	1.800	3.900	2.5	$<2.30 \times 10^{12}$
...	...	c	0.060	0.130	...	...
HD 128311	16.32	b	1.769	1.084	4.6	$<4.40 \times 10^{12}$
...	...	c	3.789	1.740	...	...
GJ 3942	16.95	b	0.022	0.061	2.4	$<2.48 \times 10^{12}$
HD 7924	17.0	d	0.020	0.155	2.9	$<3.01 \times 10^{12}$
...	...	c	0.025	0.113	...	...
...	...	b	0.020	0.060	...	...
ρ CrB	17.51	b	1.093	0.224	3.0	$<3.30 \times 10^{12}$
...	...	c	0.089	0.421	...	...
...	...	d	0.068	0.827	...	...
...	...	e	0.012	0.106	...	...

ORCID iDs

Kevin N. Ortiz Ceballos https://orcid.org/0000-0003-3455-8814
Yvette Cendes https://orcid.org/0000-0001-7007-6295
Edo Berger https://orcid.org/0000-0002-9392-9681
Peter K. G. Williams https://orcid.org/0000-0003-3734-3587

References

Acharya, A., Kashyap, V. L., Saar, S. H., Singh, K. P., & Cuntz, M. 2023, ApJ, 951, 152
Antonova, A., Doyle, J. G., Hallinan, G., Golden, A., & Koen, C. 2007, A&A, 472, 257
Astudillo-Defru, N., Forveille, T., Bonfils, X., et al. 2017, A&A, 602, A88
Bastian, T., Dulk, G., & Leblanc, Y. 2000, ApJ, 545, 1058
Bastian, T. S., Villadsen, J., Maps, A., Hallinan, G., & Beasley, A. J. 2018, ApJ, 857, 133
Ben-Jaffel, L., Ballester, G. E., Muñoz, A. G., et al. 2021, NatAs, 6, 141
Benz, A. O., & Guedel, M. 1994, A&A, 285, 621
Berger, E. 2002, ApJ, 572, 503
Berger, E. 2006, ApJ, 648, 629
Berger, E., Ball, S., Becker, K. M., et al. 2001, Natur, 410, 338
Berger, E., Rutledge, R. E., Phan-Bao, N., et al. 2009, ApJ, 695, 310
Berger, E., Rutledge, R. E., Reid, I. N., et al. 2005, ApJ, 627, 960
Blanco-Pozo, J., Perger, M., Damasso, M., et al. 2023, A&A, 671, A50
Boudreaux, T. M., Newton, E. R., Mondrik, N., Charbonneau, D., & Irwin, J. 2022, ApJ, 929, 80
Bower, G. C., Bolatto, A., Ford, E. B., & Kalas, P. 2009, ApJ, 701, 1922
Braun, R., Bonaldi, A., Bourke, T., Keane, E., & Wagg, J. 2019, arXiv:1912.12699
Burke, B. F., & Franklin, K. L. 1955, JGR, 60, 213
Callingham, J. R., Vedantham, H. K., Shimwell, T. W., et al. 2021, NatAs, 5, 1233
Cauley, P. W., Shkolnik, E. L., Llama, J., & Lanza, A. F. 2019, NatAs, 3, 1128
Cendes, Y., Williams, P. K. G., & Berger, E. 2021, AJ, 163, 15
Christensen, U. R., Holzwarth, V., & Reiners, A. 2009, Natur, 457, 167
Climent, J. B., Guirado, J. C., Pérez-Torres, M., Marcaide, J. M., & Peña-Moñino, L. 2023, Sci, 381, 1120
Cuntz, M., Saar, S. H., & Musielak, Z. E. 2000, ApJL, 533, L151
Desch, M. D., & Kaiser, M. L. 1984, Natur, 310, 755
Driessen, L. N., Heald, G., Duchesne, S. W., et al. 2023, PASA, 40, e036
Dulk, G. A. 1985, ARA&A, 23, 169
Durney, B. R., De Young, D. S., & Roxburgh, I. W. 1993, SoPh, 145, 207
Farrish, A. O., Alexander, D., Maruo, M., et al. 2019, ApJ, 885, 51
Gaia Collaboration, Prusti, T., de Bruijne, J. H. J., et al. 2016, A&A, 595, A1
Gaia Collaboration, Vallenari, A., Brown, A. G. A., et al. 2023, A&A, 674, A1
Gao, Y., Qian, L., & Li, D. 2020, ApJ, 895, 22

Gloudemans, A. J., Callingham, J. R., Duncan, K. J., et al. 2023, A&A, 678, A161
Guedel, M., & Benz, A. O. 1993, ApJL, 405, L63
Gurdemir, L., Redfield, S., & Cuntz, M. 2012, PASA, 29, 141
Hallinan, G., Bourke, S., Lane, C., et al. 2007, ApJL, 663, L25
Hallinan, G., Littlefair, S. P., Cotter, G., et al. 2015, Natur, 523, 568
Hori, Y. 2021, ApJ, 908, 77
Hughes, A. G., Boley, A. C., Osten, R. A., White, J. A., & Leacock, M. 2021, AJ, 162, 43
Kao, M. M., Hallinan, G., Pineda, J. S., Stevenson, D., & Burgasser, A. 2018, ApJS, 237, 25
Kao, M. M., Hallinan, G., Pineda, J. S., et al. 2016, ApJ, 818, 24
Kao, M. M., Mioduszewski, A. J., Villadsen, J., & Shkolnik, E. L. 2023, Natur, 619, 272
Kao, M. M., & Sebastian Pineda, J. 2022, ApJ, 932, 21
Kavanagh, R. D., Vidotto, A. A., Klein, B., et al. 2021, MNRAS, 504, 1511
Lacy, M., Baum, S. A., Chandler, C. J., et al. 2020, PASP, 132, 035001
Lazio, T. J. W., Carmichael, S., Clark, J., et al. 2009, AJ, 139, 96
Lazio, T. J. W., & Farrell, W. M. 2007, ApJ, 668, 1182
Lazio, T. J. W., Farrell, W. M., Dietrick, J., et al. 2004, ApJ, 612, 511
Lecavelier des Etangs, A., Sirothia, S. K., Gopal-Krishna, & Zarka, P. 2011, A&A, 533, A50
Lecavelier des Etangs, A., Sirothia, S. K., Gopal-Krishna, & Zarka, P. 2013, A&A, 552, A65
Lynch, C., Murphy, T., Kaplan, D., Ireland, M., & Bell, M. 2017, MNRAS, 467, 3447
McLean, M., Berger, E., & Reiners, A. 2012, ApJ, 746, 23
McMullin, J. P., Waters, B., Schiebel, D., Young, W., & Golap, K. 2007, in ASP Conf. Ser. 376, Astronomical Data Analysis Software and Systems XVI, ed. R. A. Shaw, F. Hill, & D. J. Bell (San Francisco, CA: ASP), 127
Merloni, A., Lamer, G., Liu, T., et al. 2024, A&A, 682, A34
Mohanty, S., Basri, G., Shu, F., Allard, F., & Chabrier, G. 2002, ApJ, 571, 469
Noyola, J. P., Satyal, S., & Musielak, Z. E. 2014, ApJ, 791, 25
Noyola, J. P., Satyal, S., & Musielak, Z. E. 2016, ApJ, 821, 97
O'Gorman, E., Coughlan, C. P., Vlemmings, W., et al. 2018, A&A, 612, A52
Parker, E. N. 1955, ApJ, 122, 293
Pérez-Torres, M., Gómez, J. F., Ortiz, J. L., et al. 2021, A&A, 645, A77
Pineda, J. S., & Hallinan, G. 2018, ApJ, 866, 155
Pineda, J. S., Hallinan, G., & Kao, M. M. 2017, ApJ, 846, 75
Pineda, J. S., & Villadsen, J. 2023, NatAs, 7, 569
Pope, B. J. S., Bedell, M., Callingham, J. R., et al. 2020, ApJL, 890, L19
Pope, B. J. S., Withers, P., Callingham, J. R., & Vogt, M. F. 2019, MNRAS, 484, 648
Reiners, A., Basri, G., & Browning, M. 2009, ApJ, 692, 538
Reiners, A., & Christensen, U. R. 2010, A&A, 522, A13
Rose, K., Pritchard, J., Murphy, T., et al. 2023, ApJL, 951, L43
Route, M. 2019, ApJ, 872, 79
Route, M., & Wolszczan, A. 2012, ApJL, 747, L22
Route, M., & Wolszczan, A. 2016, ApJ, 830, 85
Route, M., & Wolszczan, A. 2023, ApJ, 952, 118
Saur, J., Grambusch, T., Duling, S., Neubauer, F., & Simon, S. 2013, A&A, 552, A119
Schreyer, E., Owen, J. E., Spake, J. J., Bahroloom, Z., & Di Giampasquale, S. 2023, MNRAS, 527, 5117
Selina, R., McKinnon, M., Beasley, A. J., et al. 2018, Proc. SPIE, 10700, 107001O
Shkolnik, E., Walker, G. A. H., & Bohlender, D. A. 2003, ApJ, 597, 1092
Shkolnik, E., Walker, G. A. H., Bohlender, D. A., Gu, P., & Kurster, M. 2005, ApJ, 622, 1075
Stelzer, B., Marino, A., Micela, G., Lopez-Santiago, J., & Liefke, C. 2013, MNRAS, 431, 2063
Stelzer, B., Schmitt, J. H. M. M., Micela, G., & Liefke, C. 2006, A&A, 460, L35
Stevenson, D. J. 2003, E&PSL, 208, 1
Treumann, R. A. 2006, A&ARv, 13, 229
Trigilio, C., Biswas, A., Leto, P., et al. 2023, arXiv: 2305.00809
Trigilio, C., Umana, G., Cavallaro, F., et al. 2018, MNRAS, 481, 217
Turner, J. D., Grießmeier, J.-M., Zarka, P., Zhang, X., & Mauduit, E. 2024, A&A, 688, A66
Turner, J. D., Zarka, P., Grießmeier, J.-M., et al. 2021, A&A, 645, A59
Turnpenney, S., Nichols, J. D., Wynn, G. A., & Burleigh, M. R. 2018, ApJ, 854, 72
van Leeuwen, F. 2007, A&A, 474, 653
Vedantham, H. K., Callingham, J. R., Shimwell, T. W., et al. 2020, NatAs, 4, 577
Villadsen, J., & Hallinan, G. 2019, ApJ, 871, 214
Williams, P. K. G. 2018, in Handbook of Exoplanets, ed. H. J. Deeg & J. A. Belmonte (Berlin: Springer), 171
Williams, P. K. G., Berger, E., & Zauderer, B. A. 2013, ApJL, 767, L30
Williams, P. K. G., Clavel, M., Newton, E., & Ryzhkov, D., 2017 pwkit: Astronomical utilities in Python, Astrophysics Source Code Library record ascl:1704.001
Williams, P. K. G., Cook, B. A., & Berger, E. 2014, ApJ, 785, 9
Winglee, R. M., Dulk, G. A., & Bastian, T. S. 1986, ApJL, 309, L59
Wright, N. J., Newton, E. R., Williams, P. K. G., Drake, J. J., & Yadav, R. K. 2018, MNRAS, 479, 2351
Zarka, P. 1998, JGRE, 103, 20159
Zarka, P. 2007, P&SS, 55, 598
Zarka, P., Bougeret, J.-L., Briand, C., et al. 2012, P&SS, 74, 156
Zarka, P., Lazio, J., & Hallinan, G. 2015, in Proc. Advancing Astrophysics with the Square Kilometre Array (AASKA14), Vol. 215 (Trieste: SISSA), 120
Zarka, P., Queinnec, J., Ryabov, B. P., et al. 1997, in Planetary Radio Emissions IV, Proc. 4th Int. Workshop, ed. H. O. Rucker, S. J. Bauer, & A. Lecacheux (Vienna: Austrian Academy of Sciences Press), 101